Available online at www.sciencedirect.com
ScienceDirect
Trans. Nonferrous Met. Soc. China 34(2024) 2367−2380
Transactions of Nonferrous Metals Society of China
www.tnmsc.cn

Electrodeposition of dendrite-free Zn on Au from deep eutectic system based on choline chloride

Vesna S. CVETKOVIĆ[1], Nebojša D. NIKOLIĆ[1],
Tanja S. BARUDŽIJA[2], Silvana B. DIMITRIJEVIĆ[3], Jovan N. JOVIĆEVIĆ[1]

1. Department of Electrochemistry, Institute of Chemistry, Technology and Metallurgy, University of Belgrade, Njegoševa 12, 11000 Belgrade, Serbia;
2. Institute for Nuclear Sciences Vinča, University of Belgrade, P.O. Box 522, 11001 Belgrade, Serbia;
3. Mining and Metallurgy Institute, Zeleni bulevar 35, 19210 Bor, Serbia

Received 9 February 2023; accepted 12 June 2023

Abstract: The electrochemical deposition of zinc/gold dendrite-free alloys was achieved from deep eutectic solvents based on a mixture of choline chloride and ethylene glycol, without using any additives. Potentiostatic electrodeposition was carried out at relatively low Zn electrodeposition overpotential at different Zn(II) concentrations. Insight into the electrochemical mechanism of the Zn electrodeposition was revealed by cyclic voltammetry (CV) and chrono-amperometry (CA). The morphology and structure of the obtained electrodeposits were characterized by scanning electron microscopy (SEM) and X-ray diffraction (XRD), while the elemental analysis was determined by energy dispersive spectroscopy (EDS) technique. The CV results showed that Zn electrodeposition commences with zinc underpotential deposition (UPD) and proceeds through the zinc overpotential deposition (OPD) region. The deposition potential of the Zn/Zn(II) couple shifts towards more positive value with increased Zn(II) concentration. CA analysis demonstrated that in the zinc OPD region, 3D progressive nucleation starts, followed by 3D growth of depositing zinc. Morphological analysis revealed that electrodeposition commences with the formation of compact Zn islands and proceeds through dendrite-free zinc/gold alloys formed. A formation of several intermetallics, namely cubic $AuZn_3$ and AuZn along with metallic zinc were identified by XRD analysis.

Key words: zinc electrodeposition; deep eutectic solvent; zinc/gold alloys; morphology; structure

1 Introduction

There is an ongoing focus on the improvement of electric energy storage devices, such as zinc/air or zinc/nickel batteries [1−3]. The key limiting factor in power density deterioration and longevity of these devices is the structure of the zinc deposit and possible dendrite formation during recharging. One of the strategies to prevent zinc dendrite formation is to incorporate changes in either the electrodes or the electrolyte [4]. Ionic liquids have been recognized as candidates to replace the conventional electrolytes for possible zinc dendrite-free electrodeposition [1,2,5]. Electrodeposition of zinc and Au/Zn alloys onto polycrystalline gold and single crystal Au(100) and Au(111) from ionic liquids, has gained significant attention in aerospace, energy storage devices and automotive industry [2,5−8]. It was also found application in producing sensors which are playing leading role in detecting the biomarkers, contaminants etc. in medicine, environmental protection, and food safety [7,9]. To enhance sensors performance, most commonly

Corresponding author: Vesna S. CVETKOVIĆ, E-mail: v.cvetkovic@ihtm.bg.ac.rs
DOI: 10.1016/S1003-6326(24)66547-7

nanoporous gold (NPG) deposits are used. One of the methods for fabricating NPG is electrochemical alloying/dealloying procedure [7]. In this electrochemical approach, the selective dissolution of less noble metals (e.g., Zn, Cu, Ag) from the alloys formed with gold leads to a higher level of control of the NPG pore dimensions and uniformity [7].

Several studies on Zn electrodeposition from room temperature ionic liquids (RTILs) have been reported. These media when prepared for Zn electrodeposition are usually composed of the metal's chloride salt, organic cation, imidazolium or pyrrolidinium cation and different anions [10−12]. BORISSOV et al [6] investigated underpotential (UPD) and overpotential (OPD) deposition of Au/Zn alloys from 1-butyl-3-methylimidazolium chloride (BMIC) ionic liquid containing dissolved $ZnCl_2$. Using the Au(111) single crystal substrate as the working electrode, they demonstrated that the zinc coating is not a mono-phase, and that it contains a mixture of zinc and several intermetallic phases, namely AuZn, $AuZn_3$, and $Au_{1.2}Zn_{8.8}$ [6]. LIU et al [10] reported electrodeposition of Zn onto Au(111) from zinc triflate ($Zn(TfO)_2$) in 1-ethyl-3-methylimidazolium trifluoromethylsulfonate ([EMIm]TfO) ionic liquid. The same researchers later investigated the influence of 1,2-dimethyl-3-(trifluoromethyl)-1H-pyrazol-2-ium trifluoromethylsulfonate additive on the electrodeposition of zinc onto gold cathode from zinc triflate $Zn(TfO)_2$ in the 1-ethyl-3-methylimidazolium trifluoromethylsulfonate ([EMIm]TfO) ionic liquid [1]. XU et al [4] showed that dendrite-free Zn can be electrodeposited from electrolyte 9 mol/L KOH + 5 wt.% ZnO, containing 0.5 wt.% of RTILs 1-ethyl-3-methylmidazolium dicyanamide [4]. DOGEL et al [13] studied the underpotential (UPD) and overpotential deposition (OPD) of Zn onto Au(111) from $AlCl_3$-1-methyl-3-butylimidazolium electrolyte containing 1 mmol Zn(II).

Relatively recently, a new class of ILs, namely the deep eutectic solvents (DESs) have been widely employed as an alternative medium for a range of metals and metal alloys electrodepositions [8]. This relatively new class of ILs became preferable not only because of their role in minimizing the impact of ambient moisture but also due to their desirable physicochemical properties [2,11,12]. In electrodeposition of metals, such as Zn, Co, Ni, Pd, Ag, Cu, Sn, or Ru, considerable attention has been dedicated to the development of effective electrolytic processes which should replace current technologies that use aqueous electrolytes, with DES electrolytes based on choline chloride and hydrogen bond donors (such as ethylene glycol, urea, and renewable carboxylic acids) [14,15]. It has been shown that DES not only combines the advantages of the system's wide electrochemical window in low temperature operation but also can provide metals and alloys that are otherwise usually electrodeposited from high temperature molten salts [15]. Electrodeposition of Zn from deep eutectic systems is mainly carried out from an electrolyte mixture composed of choline chloride (ChCl):ethylene glycol (EG) or ChCl:Urea containing $ZnCl_2$ [8,12,15,16]. ABBOT et al [16] studied the electrodeposition of Zn from ChCl:EG and ChCl:Urea DESs onto a platinum disc working electrode. They found that different chloride activities in the electrolytes changed the concentration of Zn in the electrochemical double layer, which influenced the altering morphology of the electrodeposited Zn. WHITEHEAD et al [17] investigated the Zn electrodeposition process by cyclic voltammetry and potential step techniques from ChCl:EG containing $ZnCl_2$ using static and rotating glassy carbon (GC) disc cathodes at 30 °C. The conductivity of the ChCl:EG (1:2) system at 40 °C is 11 mS/cm, which proved to be much higher compared to the room temperature ionic liquids system [14,17]. For the study of the voltammetric behavior of the 0.3 mol/L $ZnCl_2$ in ChCl:EG, VIEIRA et al [18] employed glassy carbon, stainless steel, Au, Pt, Cu, and Zn working electrodes. They showed that the electrodeposition of Zn occurs through the formation of an intermediate zinc species and its subsequent reduction to Zn [18]. ISMAIL [12] reported the influence of the additive methyl nicotinate (MN) on the electrodeposition process of zinc on a copper substrate from a ChCl:EG and in a more recent study CHEN et al [19] investigated the corrosion resistance of zinc coatings deposited on mild steel from ChCl:EG [19]. Also, in the literature, there are number of reports showing that highly homogeneous and flat zinc deposits can be obtained under the influence of additives to the electrolytes used [5,11,12,20].

Previous investigations have mainly addressed the electrodeposition of Zn in zinc−chloride ILs or from Lewis acid melt systems, on different substrates in the underpotential (UPD) and overpotential deposition (OPD) regions. The study of the electrochemical deposition and nucleation mechanism of Zn metal on polycrystalline gold from an ionic liquid comprising ChCl+EG+$ZnCl_2$ have not been reported yet. This is the first study on the Zn electrodeposition onto polycrystalline gold electrode from 1:2 ChCl:EG electrolyte at 60 °C. One of tasks to be fulfilled is answer to the possibility of achieving a dendrite-free Zn deposition without using additives. Furthermore, the phase composition of the Au/Zn alloys formed by electrochemical deposition of zinc onto gold from a ChCl:EG at 60 °C should be defined and the influence of the deposition potential on the morphology of deposited Zn will be highlighted.

2 Experimental

A mixture consisting of choline chloride (≥98%, $HOC_2H_4N(CH_3)_3Cl$, ChCl) and ethylene glycol (99.8%, ethane-1,2-diol, EG) was prepared by mixing ChCl and EG at a 1:2 molar ratio. The mixture was then placed onto a hot plate for 2.5 h at 40 °C, and slowly mixed under argon atmosphere until a homogeneous colorless liquid was formed. The electrolytes containing $ZnCl_2$ (0.01 mol/L, 0.1 mol/L and 0.5 mol/L) were made by adding zinc chloride (99.999% $ZnCl_2$), to the prepared mixture. The electrolyte was stirred again under the argon atmosphere until all the salt was dissolved. Finally, the electrolyte was transferred to a three-electrode electrochemical cell supplied with argon atmosphere and subsequent experiments were done without rigorous control of the moisture. All chemicals were purchased from Sigma Aldrich, (Burlington, MA, US), and used without additional purification. The electrochemical cell used for the experiments was made of Pyrex glass to enable visual insight into the system. All experiments were performed at 60 °C. Gold (Au, 99.999%) wires and plates were used as the working electrodes for electrochemical measurements and deposition processes. To maintain constant Zn concentration in the bulk electrolyte, a zinc plate (active surface area in the electrolyte 7.5 cm^2, Zn 99.99%) was used as a counter electrode. As a reference electrode, a Zn rod (Zn, d=3 mm, 99.99%) was used. The electrode materials were purchased from Alfa Aesar (Haverhill, MA, USA). Before the experiments, gold electrodes were etched in aqua regia (1:3 HNO_3+HCl), rinsed with deionized water and absolute ethyl alcohol and dried before use. Zn electrodes were etched in a solution made of HNO_3+H_2O, (volume ratio 1:10), rinsed with deionized water and absolute ethyl alcohol and dried before use.

For all electrochemical measurements: cyclic voltammetry (CV, using various scan rates in the range of 2−20 mV/s), chronoamperometry (CA), potentiodynamic and open-circuit potential measurements, at working temperature of 60 °C, a potentiostat/galvanostat Interface 1010 E (Gamry Instruments, Warminster, PA, US) was used. Electrodeposition of Zn was performed by applying constant potentials at the Au cathode in the electrolytes containing different Zn^{2+} concentrations. All working electrode potentials were measured with respect to the potential of the zinc reference electrode, the Zn/Zn^{2+}couple.

The morphology and composition of Zn deposits electrodeposited at 0.100 V and −0.100 V vs Zn were explored using a scanning electron microscope (SEM, JOEL JSM−IT300LV), equipped with an energy-dispersive X-ray spectroscopy (EDS) Oxford Instruments X-MAX^N and AZtec version 3.1 software. The specifications of SEM and EDS analysis were: acceleration voltage 20 keV, spot size 60, probe current 2 nA, WD 10 mm, in high vacuum mode using back scattered electron and secondary detector. The crystalline structure of the deposits was analyzed by X-ray diffraction employing a SmartLab® X-ray diffractometer (Rigaku Co., Tokyo, Japan), with Cu K_α radiation at a continuous scanning mode (40 kV, 30 mA, and λ=1.542 Å) and scanning rate of 0.5 (°)/min. Phases formed during deposition were identified by a comparison to the standard reference X-ray powder diffraction patterns for phase identification, Joint Committee on Powder Diffraction Standards (JCPDS) database.

3 Results and discussion

3.1 Electrochemical measurements

Figure 1 presents typical CVs for the deposition and dissolution of Zn recorded on a

polycrystalline Au electrode immersed in ChCl:EG with different $ZnCl_2$ concentrations at 60 °C. The working temperature of the system (60 °C) was based on the previous studies on the electro-depositions of Zn from ILs at working temperatures up to 80 °C [12].

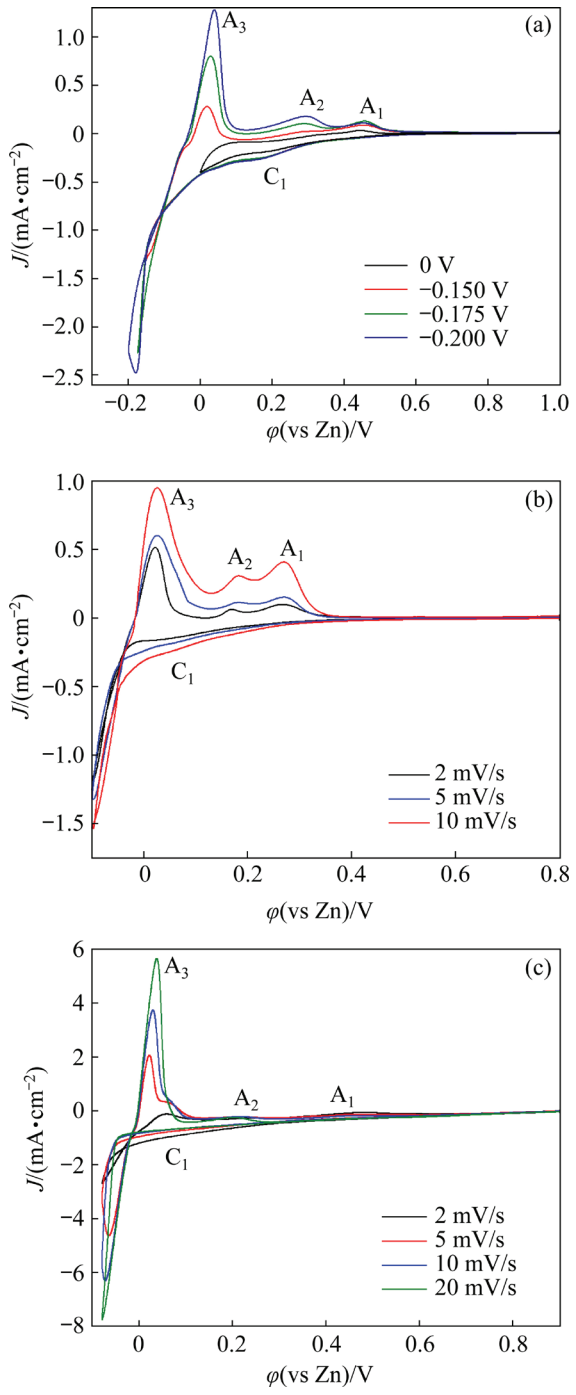

Fig. 1 Cyclic voltammograms of Au cathodes in choline chloride:ethylene glycol (1:2 molar ratio) electrolyte containing different concentrations of $ZnCl_2$: (a) 0.01 mol/L $ZnCl_2$ (scan rate: 10 mV/s); (b) 0.1 mol/L $ZnCl_2$; (c) 0.5 mol/L $ZnCl_2$ (All CVs were recorded at 60 °C)

Within the potential range explored, the CV started from the initial potential, slightly negative to the working electrode open circuit potential (OCP), towards a final chosen cathodic potential and then back to the initial potential in the reverse scan. Scanning was done using different scan rates. During the cathodic scan in the Zn underpotential region (UPD) region, one reduction (C_1) and one oxidation (A_1) current waves were observed, as shown in Figs. 1(a−c). Peak potential of C_1 appeared at about 0.170 V vs Zn, and that of its anodic counterpart at about 0.420 V vs Zn. This pair of current waves should be attributed to the underpotential deposition and dissolution of Zn, most likely accompanied by the formation of Au/Zn alloys. There are recent reports on a deposition from similar electrolyte done onto Au(111) and Au(100) single crystal surfaces and the current peak at about 0.200 V vs Zn was also attributed to Zn UPD and Au/Zn surface alloy formation [21].

At Zn overpotentials negative to about −0.050 V vs Zn, classical nucleation and electro-crystallization current loops indicating the deposition of the Zn bulk metal were recorded. These nucleation and electro-crystallization loops have been often reported for Zn deposited on a foreign substrate from ionic liquid electrolyte media [11]. The monomeric tetrachlorozincate $[ZnCl_4]^{2-}$ complexes are the main Zn containing species in the used electrolyte and the electro-deposition of zinc takes place from these species. These complex species appear to affect both, the trend in deposition potential of the Zn/Zn(II) couple shifting its potential, and the kinetics of the deposition/stripping process. With increasing Zn^{2+} concentration in the electrolyte, the beginning of the current loops was shifted to less negative electrode potentials. In the 0.01 mol/L $ZnCl_2$ electrolyte, the start of the nucleation loop was observed at potential of about −0.150 V (Fig. 1(a)), in 0.1 mol/L $ZnCl_2$ at about −0.100 V (Fig. 1(b)), and in 0.5 mol/L $ZnCl_2$ at potentials around −0.060 V vs Zn (Fig. 1(c)). No voltammogram recorded for the cathodic end potential values being less negative than about −0.175 V vs Zn has shown diffusion-controlled Zn deposition. The diffusion-controlled Zn bulk deposition in the voltammograms becomes obvious only at the cathodic end potentials applied above −0.200 V vs Zn, even in the least concentrated 0.01 mol/L electrolyte. In the

reverse scan, the deposited Zn bulk metal is anodically dissolved, which is designated by the clearly defined anodic current peak A_3. Dissolution of the zinc from Au/Zn alloys formed during deposition is reflected by the A_2 peak. The anodic peak A_1 in Fig. 1 should be associated with the dissolution of Zn from underpotentially deposited Zn and from Au/Zn alloys synthetized during Zn UPD. It appears that there was more than one intermetallic formed in the Zn OPD and UPD region, being reflected by stripping peaks A_2 and A_1, which would explain two intermetallics having different dissolution potentials [22−24]. Similar voltametric results have previously been recorded in the investigation of Zn UPD and OPD deposition on gold Au(111) substrate from $ZnCl_2$−BMIC ionic liquid [6]. Careful observation of the reverse scan of the voltammogram obtained with a scan rate of 5 mV/s in Fig. 1(c)), revealed that there is a small shoulder at the potential of about 0.100 V vs Zn. This small shoulder was observed only once in this study. The appearance of this shoulder is often seen on the CVs recording Zn electrodeposition and dissolution on a working substrate in different ionic liquids. In most of the cases, the so-called peak is not addressed [10,21]. However, when the appearance of this peak is addressed, it is attributed to dissolution of electrodeposited Zn metal [11,19].

Figures 2(a, b) display the CVs performed on the Au polycrystalline surface with varying cathodic end scan limits for two electrolytes of different $ZnCl_2$ concentrations, 0.01 mol/L (Fig. 2(a)) and 0.1 mol/L (Fig. 2(b)), respectively. When the CV obtained with the cathodic end potential of 0 V was compared to the CV with the cathodic end potential of −0.150 V vs Zn under the same conditions, the stripping current peak (A_1) in both examples was clearly defined and located at about 0.350 V vs Zn. It is apparent that the stripping current peak A_1 reflects the dissolution of Au/Zn alloys, which in turn confirms that during the Zn underpotential deposition, Au/Zn alloys are formed. To get further insight into the Zn UPD, the system was investigated by applying different holding times at the cathodic end potentials (e.g., 0.100 V vs Zn) slightly negative to cathodic current peak C_1 potential, in the electrolytes having different $ZnCl_2$ concentrations, 0.1 and 0.5 mol/L (Figs. 3(a, b)). The results presented in Fig. 3 suggest that the applied cathodic end potential of 0.100 V vs Zn induces Zn UPD deposition from the electrolytes of both Zn(II) concentrations. This was supported by the increase in cathodic and anodic currents, including the charges encompassed by the cathodic and anodic current waves, with increased deposition time. Within anodic current waves, the increase in charge with increased deposition time indicates more zinc/gold being dissolved. However, there are two characteristics that should be addressed. First, under all other experimental conditions keeping the same, the maximum deposition and dissolution currents remained practically the same when the deposition time was doubled. Second, the charge limited by anodic currents, as well as that limited by cathodic currents, remained practically the same when the zinc concentration in the electrolyte was increased five times.

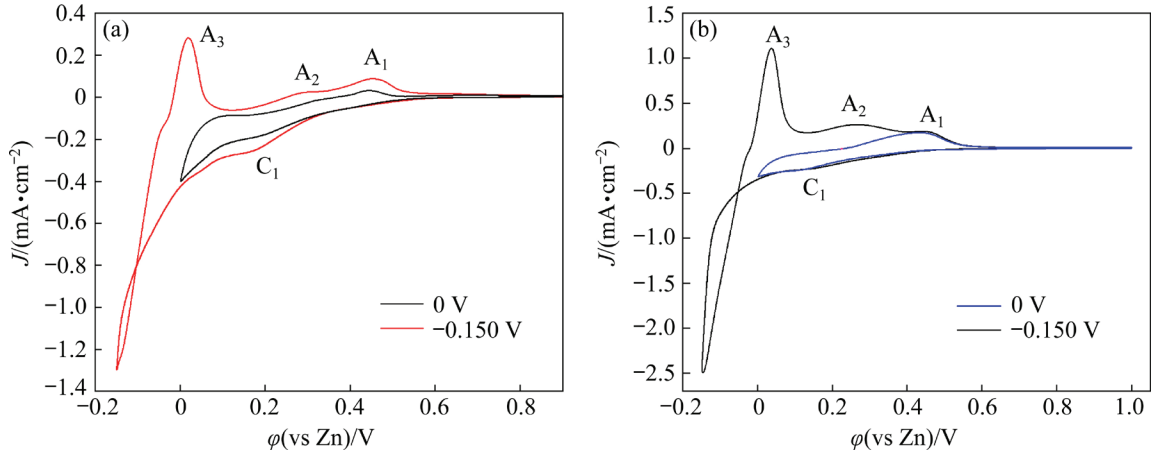

Fig. 2 Cyclic voltammograms on Au cathodes in choline chloride:ethylene glycol (1:2 molar ratio) electrolyte containing different concentrations of $ZnCl_2$: (a) 0.01 mol/L $ZnCl_2$; (b) 0.1 mol/L $ZnCl_2$ (Potential change started from φ_i=0.900 V or 1.000 V towards different φ_c and back to φ_i with a scan rate of 10 mV/s; All CVs were recorded at 60 °C)

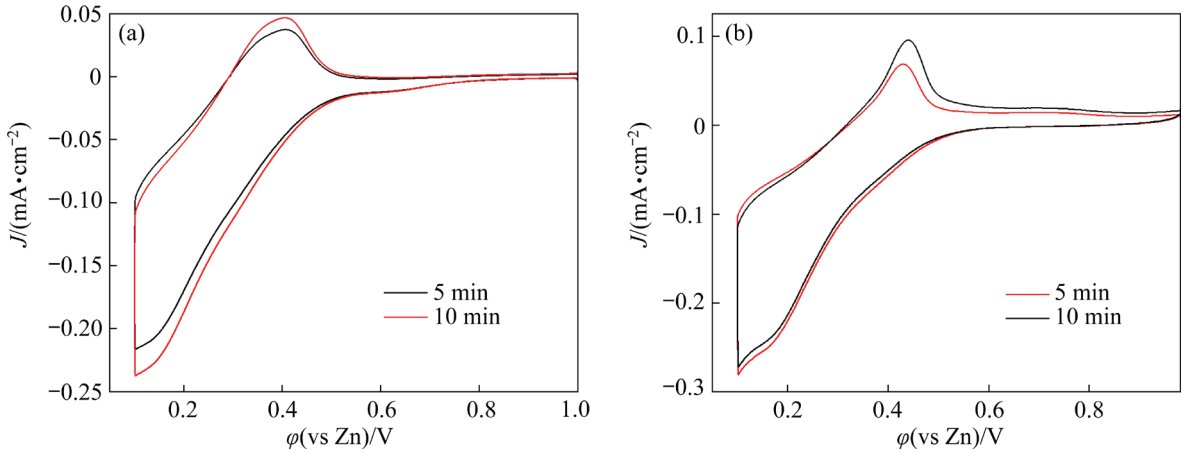

Fig. 3 Voltammograms obtained from Au working electrode by holding at potential of 0.100 V vs Zn in choline chloride:ethylene glycol (1:2 molar ratio) electrolyte containing different concentrations of $ZnCl_2$: (a) 0.1 mol/L; (b) 0.5 mol/L (Working temperature: 60 °C; holding time: 5 and 10 min; scan rate: 10 mV/s)

Furthermore, under the same conditions, the charge limited by anodic current waves was smaller than that under its cathodic counterparts. This is an indication that the alloy formation between the UPD deposited Zn and the Au substrate, exhibit some irreversibility of the deposition/dissolution process [21]. It seems that all of the zinc engaging into forming the surface Au/Zn alloys, does not leave the intermetallic to be dissolved.

This type of behavior has been observed previously in similar investigations of Zn UPD deposition from different ionic liquids [10,13,21]. Based on these previous observations, under the assumption of an UPD, the Zn coverage on both Au(111) and Au(100) substrates was estimated to be 0.41 monolayers (ML) [21]. These values were calculated from charge density, which was estimated by the integration of current density over measurement time, and divided by 2 (number of exchanged electrons per Zn atom deposited) [21]. Underpotentially deposited zinc monolayers are sources for Au/Zn surface alloys formation. Some earlier in-situ STM results suggested that complete dissolution of formed alloys is kinetically hindered, which explains the poor reversibility of the system [21]. In addition, the zinc dissolution is suppressed by the formation of Zn(II) coordinated species from dissolved Zn^{2+} ions at the electrode surface vicinity in IL electrolytes [21].

3.2 Zn nucleation on Au cathode

The chronoamperometry technique was applied to examining the nucleation mechanisms for Zn deposition from ChCl:EG onto a polycrystalline gold substrate. This technique was performed by stepping the working potential from 0.700 V vs Zn, where no reduction occurred, to different chosen cathodic end potentials that are sufficiently negative to trigger the nucleation process and Zn bulk deposit growth. The idea was to find the zinc overpotential value high enough to secure bulk zinc being deposited without diffusion control, to obtain the bulk deposit without dendrites. The current density−time responses to such probes are presented in Fig. 4. The elecro-crystallization process of bulk metal phases on the substrate made of other metals very often starts as three-dimensional (3D) nucleation and proceeds as 3D growth [25,26]. In this case, the first part of every $J=f(t)$ response to the applied overpotential, after short duration of capacitive charge, includes the current density rise reflecting the increase of the surface area of the newly born crystal and its enlargement due to further growth of the crystal. This relatively simple relationship ends at the point in time when conditions in the electrolyte (concentration of the depositing species, diffusion coefficient of the deposition species, and intensity of the possible forced diffusion, etc) reach the limiting values, thus governing diffusion-controlled deposition. These $J=f(t)$ functions have been a subject of many successful investigations ending with a selection of formulae describing every individual case of nucleation and growth with and without diffusion control [27−29]. The nucleation processes at its very beginning (instantaneous and

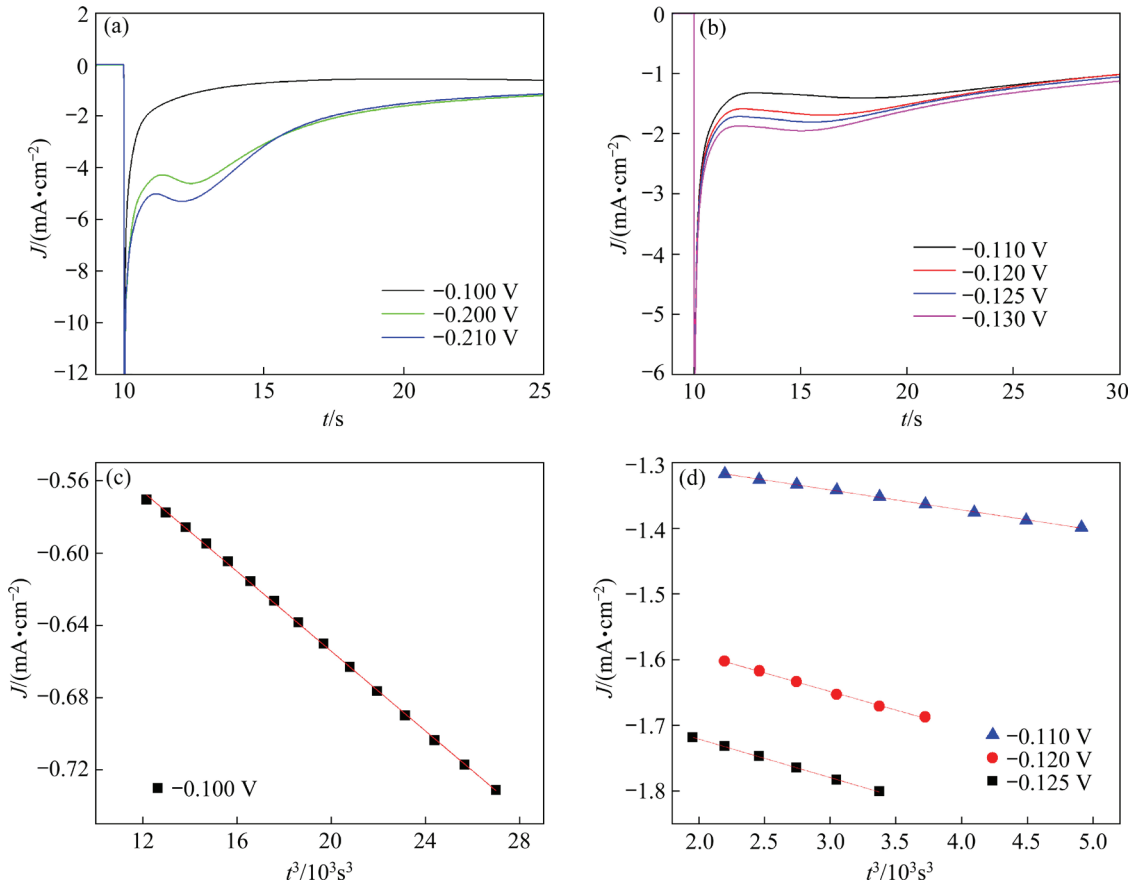

Fig. 4 Current density−time transients recorded on Au electrode at different cathodic overpotentials applied from choline chloride:ethylene glycol (1:2 molar ratio) electrolyte containing 0.1 mol/L $ZnCl_2$ at 60 °C (a, b); $J=f(t^3)$ plots obtained from J–t transients (c, d)

progressive) and consequent 3D-growth (without diffusion control of the process), were described in detail [25,26]. According to the criteria given by RANGARAJAN [30] and BUDEVSKI et al [25], the initial rising segments of the J–t transients, before they reach point in time where diffusion control becomes of crucial influence to the deposition process reflecting 3D progressive nucleation, behave according to Eq. (1):

$$J_{\text{free}} = -\frac{2}{3}\pi\frac{zF}{V_{\text{m}}} Jv^3t^3 \quad (1)$$

where: J_{free} represents the current density, z is a number of electrons exchanged, F is the Faraday constant, V_{m} is the molar volume, $J(=\text{d}Z_{\text{nuc}}/\text{d}t)$ is the nucleation rate, v is the growth rate in the case of hemispherical growth, and t is time.

The initial deposition current density increases recorded are presented in Figs. 4(a, b). Plotting the values of the initial current density from the experimental $J=f(t)$ transients obtained, in the form of the $J=f(t^3)$ relationship revealed linear dependence in accordance with Eq. (1), as shown in Figs. 4(c, d). This relationship indicates that the zinc deposition onto the Au electrode from used electrolyte starts with 3D Zn progressive nucleation and proceeds as 3D growth. In a recent study, the same conclusion was proposed by SMITH et al [31]. The authors have investigated initial nucleation process of the Zn metal deposition onto a polished gold-coated quartz crystal from ChCl:EG. The chronoamperometric measurements coupled with real time in-situ monitoring of surface structure (atomic force microscopy, AFM) and mass changes (electrochemical acoustic impedance QCM) were carried out and demonstrated that in the initial phase of Zn deposition the nucleation initially occurred as a 3D progressive nucleation [31].

3.3 Surface characterization

3.3.1 SEM and EDS analysis

The Zn electrodeposition processes were characterized by SEM analysis of the deposits obtained from 0.1 and 0.5 mol/L Zn(II) concentration

in the electrolyte. For concentrations of Zn(II) ions of 0.010 mol/L, Zn metal was not detected by EDS technique.

Figure 5 shows surface morphologies obtained by electrodeposition from 0.1 mol/L Zn(II) at an underpotential of 0.100 V (Figs. 5(a, b)), and at an overpotential of −0.100 V vs Zn (Figs. 5(c, d)).

The EDS spectra for these electrodeposits (taken from the place in orange color on SEM micrographs) are shown in Fig. 6. The presence of Au, Zn and O was detected in them, and their contents are summarized in Table 1. The values in Table 1 are given as average values of minimum three measurements.

In the electrodeposit obtained under the underpotential conditions (Figs. 5(a, b)), Zn was only detected in traces (about 1.275 wt.%). EDS analysis showed the presence of Zn only on edges of pretty regular rhomboids (Fig. 5(b)). In the electrodeposit obtained under the overpotential conditions (Figs. 5(c, d)), the content of electrodeposited Zn was considerably larger (about 8.97 wt.%) than that obtained at the underpotential deposition. This deposit is characterized by irregular compact islands, around which a relatively non-uniform deposit was formed.

The morphology of the deposit obtained by electrodeposition from 0.5 mol/L Zn is shown in Figs. 7(a, b). The compact and uniform dendrite-free electrodeposit was formed under these electrodeposition conditions.

The EDS spectrum of the electrodeposit obtained from this electrolyte is shown in Fig. 8, while results of elemental analysis are added to Table 1. In this electrodeposit, Zn is detected in noticeable quantity (about 1/3 overall mass fraction). Formation of the compact and uniform surface area which is accompanied by the high content of Zn is clear proof that compact parts of the surface area of the electrodeposits can be attributed to Zn deposition and probably Au/Zn alloys formation.

Regarding the fact that the compact dendrite-free deposit is characterized by the high content of Zn (Fig. 7), and the fact that the deposit obtained under underpotential conditions has negligible content of Zn (Figs. 5(a, b)), it is clear that compact islands obtained from 0.1 mol/L Zn(II) at −0.100 V vs Zn (Fig. 5(d))) can be attributed to dominant Zn deposition and probably Au/Zn alloys formation.

It is necessary to point out that the cathodic potential of −0.100 V vs Zn did not belong to the

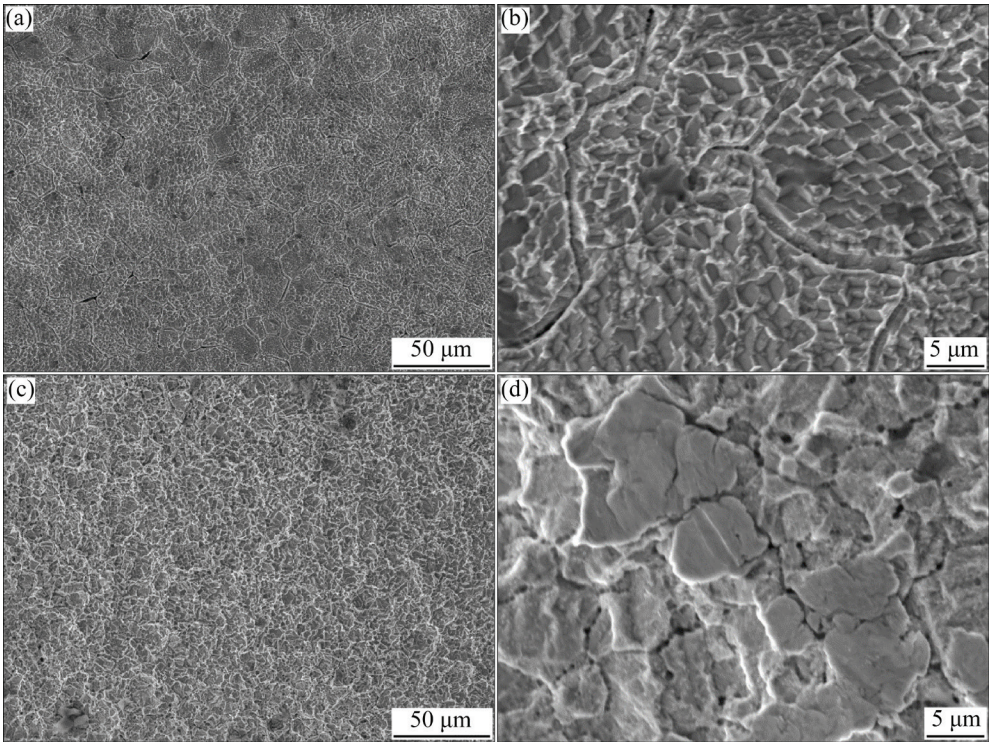

Fig. 5 SEM micrographs of deposits obtained by electrodeposition from 0.1 mol/L Zn(II): (a, b) In underpotential region (0.100 V vs Zn); (c, d) In overpotential region (−0.100 V vs Zn) (In both cases, electrodeposition time was 10 min)

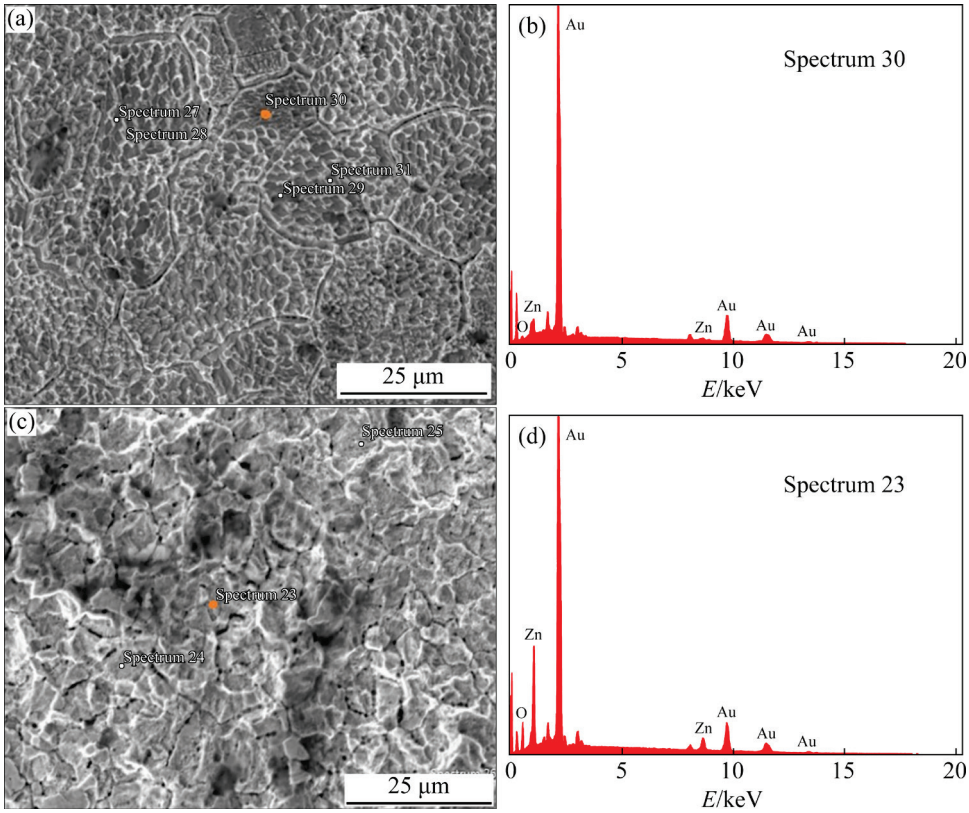

Fig. 6 SEM micrographs and EDS spectra of electrodeposits obtained from 0.1 mol/L Zn(II): (a, b) In underpotential region (0.100 V vs Zn); (c, d) In overpotential region (−0.100 V vs Zn)

Table 1 Elemental contents of electrodeposits obtained under various electrodeposition conditions (wt.%)

Electrodeposition condition	Au	Zn	O
0.1 mol/L; 0.100 V vs Zn	97.425±0.40	1.275±0.80	1.30±0.010
0.1 mol/L; −0.100 V vs Zn	83.56±2.0	8.97±0.80	7.47±0.90
0.5 mol/L; −0.100 V vs Zn	63.22±5.0	32.72±6.0	4.06±1.0

diffusion control for all used Zn electrolyte concentrations (Figs. 1(a−c)). The use of higher concentration of Zn(II) (0.5 mol/L) in the electrolyte enabled us to obtain compact and uniform deposit, while relatively non-uniform deposit with compact islands was obtained from the electrolyte containing 0.1 mol/L Zn(II). As already mentioned, elemental analysis of the electrodeposits obtained under various electrodeposition conditions indicated the formation of Au/Zn alloys, and for that reason, the further characterization of these electrodeposits by the XRD technique was done.

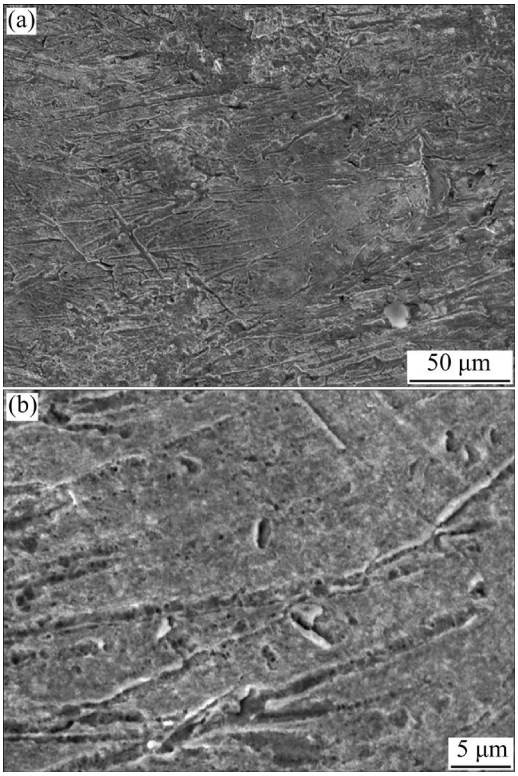

Fig. 7 SEM micrographs of deposits obtained by electrodeposition from 0.5 mol/L Zn(II) at overpotential of −0.100 V vs Zn (The electrodeposition time: 3 min)

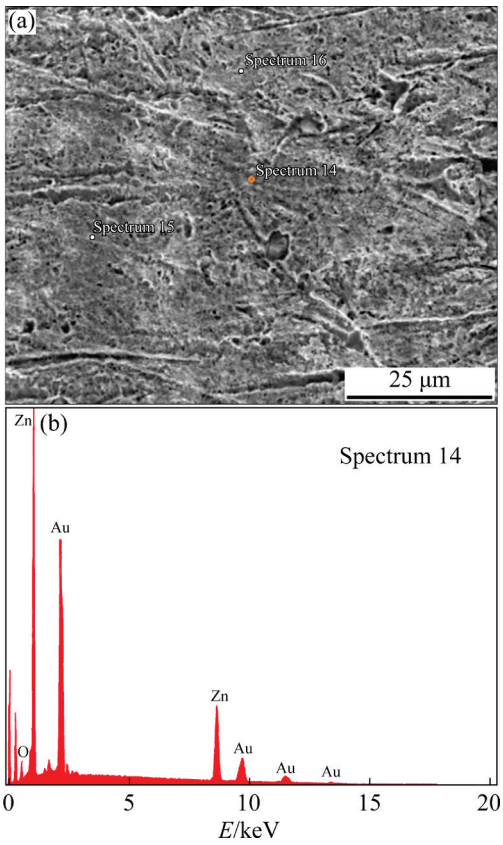

Fig. 8 SEM micrograph and EDS spectrum of electrodeposit obtained from 0.5 mol/L Zn(II) at overpotential of −0.100 V vs Zn

3.3.2 XRD analysis

X-ray diffraction analysis in this study revealed that with the metallic bulk Zn deposited from 0.1 and 0.5 mol/L $ZnCl_2$ electrolyte, several distinct intermetallics, AuZn and $AuZn_3$ phases, were formed by Zn potentiostatic deposition onto the Au polycrystalline substrate in the Zn OPD region at −0.100 V vs Zn. The results of XRD analysis of the samples formed by electrodeposition of Zn onto Au cathode in a potentiostatic mode from choline chloride:ethylene glycol (1:2 molar ratio) electrolyte containing different concentrations of $ZnCl_2$ are presented in Fig. 9.

The XRD results for the samples prepared by zinc electrodeposition from the electrolyte with 0.1 mol/L and with 0.5 mol/L $ZnCl_2$ concentration appeared to be very similar. The distinct diffraction peaks at 2θ=22.5°, 25.20°, 27.65°, 32.03°, 41.17°, 42.83°, 45.94°, 47.44°, 53.11°, 54.47°, 63.39° and 71.66° with (200), (210), (211), (220), (320), (321), (004), (014), (124), (233), (025) and (006) reflections in the diffractograms recorded were recognized as the characteristic peaks of cubic $AuZn_3$ phase [JCPDS No. 00-50-1336]. The peaks identified at 2θ=28.40°, 40.59°, 50.28°, 58.76°, 66.53°, and 73.86° with (100), (110), (111), (200), (210) and (211) were assigned to the reflections corresponding to cubic AuZn [JCPDS No. 03-065-0436].

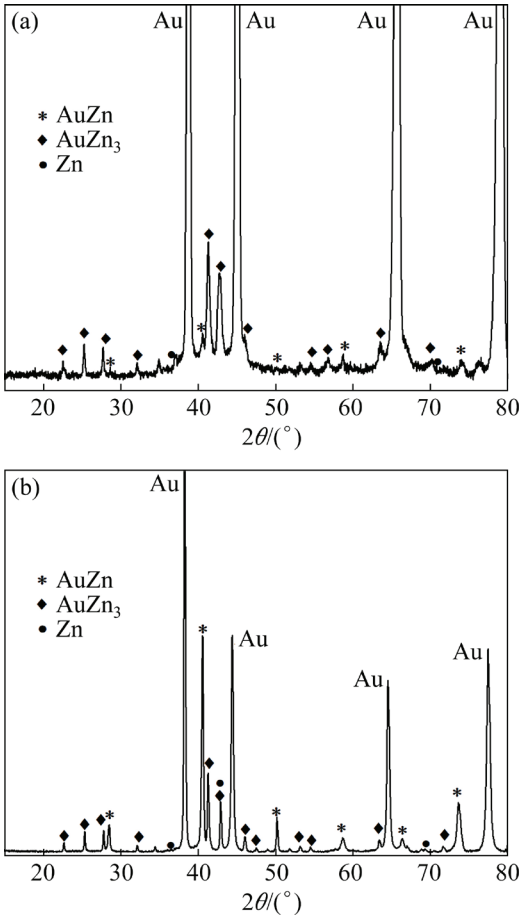

Fig. 9 X-ray diffraction patterns of deposit obtained by Zn electrodeposition in potentiostatic mode (deposition potential of −0.100 V vs Zn) from choline chloride: ethylene glycol (1:2 molar ratio) electrolyte containing different concentrations of $ZnCl_2$: (a) 0.1 mol/L $ZnCl_2$, and deposition time 10 min; (b) 0.5 mol/L $ZnCl_2$, and deposition time 3 min (Working temperature: 60 °C)

Apart from the prominent peaks corresponding to AuZn and $AuZn_3$ alloys, the XRD data indicated the peaks of metallic Zn, 2θ peaks at 36.29° and 70.07 ° with reflections (002) and (103) [JCPDS No. 01-087-0713], and the peaks of the Au substrate at 2θ=38.18°, 44.38°, 64.57° and 77.56° [JCPDF No. 03-065-2870].

Our XRD findings are in agreement with the literature which names the cubic $AuZn_3$ and AuZn, as well as the hexagonal $Au_{1.2}Zn_{8.8}$ as the main

alloys of gold and zinc [21]. At 50 at.% zinc, the β'-AuZn phase is formed whereas at 75 at.% of Zn, γ_2-$AuZn_3$ is found. These two phases retain cubic structures. At zinc concentrations higher than 75 at.%, the Au/Zn alloys exhibit a transformation to hexagonal closed packed (hcp) structure, and accordingly the $Au_{1.2}Zn_{8.8}$ phase has a hexagonal structure [6]. The characteristics of XRD patterns of Au/Zn alloys formed by Zn electrodeposition on Au(111) from 1-butyl-3-methylimidazolium chloride containing $ZnCl_2$ presented by BORISSOV et al [6], and XRD data disclosed by SCHUETT et al [21] regarding the electrochemical deposition of Zn onto Au(100) and Au(111) from the ionic liquid N-methyl-N-propylpiperidinium bis(trifluoromethanesulfonyl)imide were in accordance with our results presented.

However, recently, it was suggested that the transition in AuZn phase at low temperature can be trigonal or rhombohedral with a very small distortion [32]. According to the binary Au−Zn phase diagram, an orthorhombic metastable phase was found in an alloy with 37.8 at.% Zn when it was rapidly cooled to room temperature after being kept at 600 °C for several hours [33].

3.4 General discussion

The results obtained in this study suggest Zn UPD and OPD deposition from the chosen electrolyte (0.01 mol/L, 0.1 mol/L and 0.5 mol/L $ZnCl_2$) and Au/Zn alloys formation made by solid state interdiffusion. To identify Au/Zn alloys formed in Zn UPD and OPD region onto gold from used electrolyte, XRD analyses of the working cathode surfaces after deposition were performed. Voltammetric studies in the UPD region and SEM analysis of the cathodes after zinc underpotential deposition at 0.100 V vs Zn in the electrolytes containing 0.1 mol/L and 0.5 mol/L $ZnCl_2$ confirm that Zn was underpotentially deposited. SEM and EDS analysis suggest presence of Zn only on the edges of fairly regular rhomboids. XRD results regarding the formation of the Au/Zn alloys by zinc underpotential deposition, however, were not convincing. Similar behavior was recorded in the case of the Al UPD onto Zn substrate from chloroaluminate melts in our earlier studies [22,34]. The characteristic peaks for Al/Zn alloys formation by Al underpotential deposition on Zn substrate from the chloroaluminate molten salts in XRD diffractograms were not observed [22,34].

Analogues results and conclusions on the subject can be found in the literature. By using scanning tunneling microscopy (STM), DOGEL and FREYLAND [13] found that in the Zn UPD region, the electrodeposited zinc islands are formed on Au(111) at potentials starting at about 0.250 V vs Zn and completion of the Zn monolayer is at about 0.160 V vs Zn. By changing the potential closer to the zinc Nernst potential value (0.100 V for example), formation of Au/Zn surface alloys was induced. These values are in very good agreement with the current peak potential C_1 in the CV presented in our study (Fig. 1).

Studies of zinc electrodeposition onto gold (111) and (100) substrates from several ionic liquids have found that UPD of zinc leads to the formation of Zn monolayers and subsequently to Au/Zn alloys [6,10,13,21,35]. LIU et al [10] stated that at the electrode potential of 0.100 V vs Zn, the island continues to grow, but the process is very slow and takes several hours to get the electrode surface fully covered. This conclusion was evidenced by in-situ STM results presented [10], and it is most probably due to solid state self-diffusions of Zn and Au and diffusion mobilities in solid solutions [21,34].

It appears that the electrodeposition of zinc in our experimental potential window starts as zinc underpotential deposition (zinc UPD) of monolayers which spread very slowly over the gold polycrystalline surface. The mechanism of solid state interdiffusion transitions causes those monolayers to form surface alloys with the substrate. These alloys are most probably dominantly metastable and therefore cannot be recognized by XRD. In these processes, zinc is deposited in amounts larger than those participating in alloy formation, and therefore remains partially on the surface as metallic zinc. When the dissolution starts, the metallic zinc from the substrate dissolves into the electrolyte, but it is moderated by the formation of zinc complexes with the components of the melt, Peak A_2 in Figs. 1(a, b), and Peak A_2 in Fig. 2(b)). The zinc from surface alloys exits at more anodic potentials, but some of it remains trapped in the surface alloys formed, Peak A_1 in Figs. 1(a, b), and Peak A_1 in Fig. 2.

In the zinc overpotential deposition region (zinc OPD), 3D progressive nucleation starts,

followed by 3D growth fed by 3D diffusion with depositing zinc. Thus, a layer of Zn deposit is built. At the initial border between the gold substrate and the deposited zinc, the bottom part of this layer forms probably stable alloys, due to solid state interdiffusion (Figs. 9(a, b)). The upper part of the layer, advancing toward the bulk of the electrolyte by accumulating new amounts of Zn, allows formation of new quantities of Au/Zn alloys probably made of metastable and less dense crystals. Towards the electrolyte, the surface of advancing layer is made probably only from zinc crystallized in its usual crystal structures, partially distorted by the underlying alloy structures. When the zinc overpotential is high enough to induce and support diffusion-controlled deposition, i.e. ruled by diffusion limiting deposition current, these surface irregularities are points of dendrite birth and growth. Figures 5−8 present the surface being without prominent surface point of elevation or deformations and therefore it does not offer precursors for dendrite generation and growth. This is the situation governing zinc deposition processes on each of the gold polycrystalline grains exposed to the used IL zinc electrolyte. This is the result of applying potentiostatic low zinc overpotential deposition at potentials below −0.110 V vs Zn. In the available literature reports, there is no similar success in avoiding dendrites being formed in zinc deposition without additives used in the electrolyte. It should also be mentioned that zinc accumulates at the gold substrate grain boundaries where its nucleation energies are favorable.

4 Conclusions

(1) A new method was presented for zinc dendrite-free electrodeposition on polycrystalline Au cathode at 60 °C from a deep eutectic solvent made of choline chloride and ethylene glycol (1:2) containing Zn(II) as a source of metal component and without additives. The increase in the Zn(II) concentration in this electrolyte shifted the onset of Zn bulk electrodeposition potential towards more positive value.

(2) The results of the electrochemical studies have shown that Zn electrodeposition commences in zinc underpotential deposition (UPD) and proceeds through the zinc overpotential deposition (OPD) region. It was found that in the zinc OPD region, 3D progressive nucleation starts, followed by 3D growth of depositing zinc.

(3) CVs results showed that at the cathodic end potential values being less negative than about −0.175 V vs Zn, no diffusion-controlled Zn deposition was reached, and thus the electrochemical potential of Zn/Zn(II) redox couple favored fabricating dendrite-free Zn/Au deposits. The deposits were made potentiostatically at different electrode potentials and different Zn(II) concentrations in the electrolytic bath. Applying relatively low Zn electrodeposition overpotential, less negative than –0.110 V vs Zn, resulted in a compact deposit comprising two distinct cubic Au/Zn intermetallics, $AuZn_3$ and AuZn, and metallic Zn.

(4) Zn was detected in traces in the underpotential conditions of electrodeposition. Formation of the deposit in the Zn OPD region starts with compact Zn islands and proceeds to the full coverage of Au electrode, by electrodeposited dendrite-free Zn, $AuZn_3$ and AuZn alloys.

CRediT authorship contribution statement

Vesna S. CVETKOVIĆ: Methodology, Investigation, Writing – Review & editing, Writing – Original draft; **Nebojša D. NIKOLIĆ:** Writing SEM and EDS morphology, Editing; **Tanja S. BARUDŽIJA:** XRD analysis; **Silvana B. DIMITRIJEVIĆ:** SEM and EDS analysis; **Jovan N. JOVIĆEVIĆ:** Writing − Review & editing, Supervision.

Declaration of competing interest

The authors declare that they have no known competing financial interests or personal relationships that could have appeared to influence the work reported in this paper.

Acknowledgments

This research has been financially supported by the Ministry of Science, Technological Development and Innovation, Serbia (No: 451-03-47/2023- 01/200026).

References

[1] LIU Z, EL ABEDIN S Z, BORISENKO N, ENDRES F. Influence of an additive on zinc electrodeposition in the ionic liquid 1-ethyl-3-methylimidazolium trifluoromethylsulfonate [J]. ChemElectroChem, 2015, 2: 1159−1163.

[2] WANG Yu-sheng, YEY Hsin-wen, TANG Yi-hsuan, KAO Chai-lin, CHEN Po-yu. Voltammetric study and electrodeposition of zinc in hydrophobic room-temperature

ionic liquid 1-butyl-1-methylpyrrolidinium bis((trifluoromethyl)-sulfonyl)imide ([BMP][TFSI]): A Comparison between Chloride and TFSI Salts of Zinc [J]. Journal of the Electrochemical Society, 2017, 164: D39−D47.

[3] SIMONS T J, MACFARLANE D R, FORSYTH M, HOWLET P C. Zn electrochemistry in 1-ethyl-3-methylimidazolium and n-butyl-n-methylpyrrolidinium dicyanamides: Promising new rechargeable Zn battery electrolytes [J]. ChemElectroChem, 2014, 1: 1688−1697.

[4] XU M, IVEY D G, QU W, XIE Z. Study of the mechanism for electrodeposition of dendrite-free zinc in an alkaline electrolyte modified with 1-ethyl-3-methylimidazolium dicyanamide [J]. Journal of Power Sources, 2015, 274: 1249−1253.

[5] WANG X, XU C, LIU H, HUANG M, REN X, WANG S, HUA Y, ZHANG Q B, RU J. Influence of chloride ion on zinc electrodeposition from choline chloride based deep eutectic solvent [J]. Ionics, 2020, 26: 1483−1490.

[6] BORISSOV D, PAREEK A, RENNER F U, ROHWERDER M. Electrodeposition of Zn and Au−Zn alloys at low temperature in an ionic liquid [J]. Physical Chemistry Chemical Physics, 2010, 12: 2059−2062.

[7] van der ZALM J, CHEN S, HUANG W, CHEN A. Review—Recent advances in the development of nanoporous au for sensing applications [J]. Journal of the Electrochemical Society, 2020, 167: 037532.

[8] MANIAM K K, PAUL S. Progress in electrodeposition of zinc and zinc nickel alloys using ionic liquids [J]. Applied Science, 2020, 10: 1−20.

[9] HOSSAIN M N, LIU Z, WEN J, CHEN A. Enhanced catalytic activity of nanoporous Au for the efficient electrochemical reduction of carbon dioxide [J]. Applied Catalysis B: Environmental, 2018, 236: 483−489.

[10] LIU Z, BORISENKO N, El ABEDIN S Z, ENDRES F. In situ STM study of zinc electrodeposition on Au(111) from the ionic liquid 1-ethyl-3-methylimidazolium trifluoromethylsulfonate [J]. Journal of Solid State Electrochemistry, 2014, 18: 2581−2587.

[11] ABBOTT A P, BARRON J C, FRISCH G, RYDER K S, SILVA A F. The effect of additives on zinc electrodeposition from deep eutectic solvents [J]. Electrochimica Acta, 2011, 56: 5272−5279.

[12] ISMAIL H K. Electrodeposition of a mirror zinc coating from a choline chloride-ethylene glycol-based deep eutectic solvent modified with methyl nicotinate [J]. Journal of Electroanalytical Chemistry, 2020, 876: 114737.

[13] DOGEL J, FREYLAND W. Layer-by-layer growth of zinc during electrodeposition on Au(111) from a room temperature molten salt [J]. Physical Chemistry Chemical Physics, 2003, 5: 2484−2487.

[14] ABBOTT A P, CAPPER G, McKENZIE K J, RYDER K S. Electrodeposition of zinc-tin alloys from deep eutectic solvents based on choline chloride [J]. Journal of Electroanalitical Chemistry, 2007, 599: 288−294.

[15] QIAN H, FU X, CHI Y, ZHANG R, ZHAN C, SUN H, ZHOU X, SUN J. Study on electrodeposition and corrosion resistance of Cu−Sn alloy prepared in ChCl−EG deep eutectic solvent [J]. Journal of Solid State Electrochemistry, 2022, 26: 469−479.

[16] ABBOTT A P, BARRON J C, RYDER K S. Electrolytic deposition of Zn coatings from ionic liquids based on choline chloride [J]. Transactions of the Institute of Metal Finishing, 2009, 87: 201−207.

[17] WHITEHEAD A H, PÖLZLER M, GOLLAS B. Zinc electrodeposition from a deep eutectic system containing choline chloride and ethylene glycol [J]. Journal of the Electrochemical Society, 2010, 157: D328−D334.

[18] VIEIRA L, SCHENNACH R, GOLLAS B. The effect of the electrode material on the electrodeposition of zinc from deep eutectic solvents [J]. Electrochimica Acta, 2016, 197: 344−352.

[19] CHEN J Y, ZHU M J, GAN M T, WANG X L, GU C D, TU J P. Rapid electrodeposition and corrosion behavior of zn coating from a designed deep eutectic solvent [J]. Metals, 2023, 13: 172.

[20] FASHU S, GU C, ZHANG J, HUANG M, WANG X, TU J. Effect of EDTA and NH_4Cl additives on electrodeposition of Zn−Ni films from choline chloride-based ionic liquid [J]. Transactions of Nonferrous Metals Society of China, 2015, 25: 2054−2064.

[21] SCHUETT F M, HEURBACH M K, MAYER J, CEBLIN M U, KIBLER L A, JACOB T. Electrodeposition of zinc onto Au(111) and Au(100) from the ionic liquid [MPPip][TFSI] [J]. Angewandte Chemie−International Edition, 2021, 60: 20461−20468.

[22] CVETKOVIĆ V S, VUKIĆEVIĆ N M, JOVIĆEVIĆ J N. Aluminium and magnesium alloy synthesis by means of underpotential deposition from low temperature melts [C]// STEVANOVIĆ J. Metals and Metal-based Electrocatalytic Materials for Alternative Energy Sources and Electronics. New York, USA: Nova Science Publisher, 2019: 371−423.

[23] RADOVIĆ B S, CVETKOVIĆ V S, EDWARDS R A H, JOVIĆEVIĆ J N. Al−Fe alloy formation by aluminium underpotential deposition from $AlCl_3$+NaCl melts on iron substrate [J]. International Journal of Materials Research, 2011, 102: 59−68.

[24] JOVIĆEVIĆ N, CVETKOVIĆ S V, KAMBEROVIĆ J Ž, JOVIĆEVIĆ N J. Al−Cd alloy formation by aluminium underpotential deposition from $AlCl_3$+NaCl melts on cadmium substrate [J]. Metallurgical and Materials Transactions B, 2013, 44, 1: 106−114.

[25] BUDEVSKI E, STAIKOV G, LORENZ W J. Electro-chemical phase formation and growth [M]. New York: John Wiley & Sons, 1996.

[26] PLETCHER D, GREEF R, PEAT R, PETER L M, ROBINSON J. Electrocrystallisation [C]//PLETCHER D, GREEF R, PEAT R, PETER L M. Instrumental Methods in Electrochemistry. New York, Cichester, Weinheim, Brisbane, Singapore, Toronto: John Wiley & Sons, 2010: 283−316.

[27] BUDEVSKI E, STAIKOV G, LORENZ W J. Electro-crystallization [J]. Electrochimica Acta, 2000, 45: 2559−2574.

[28] BEWICK A, FLEISCHMANN M, THIRSK H R. Kinetics of the electrocrystallization of thin films of calomel [J]. Transactions of Faraday Society, 1962, 58: 2200−2216.

[29] CVETKOVIĆ V S, VUKIĆEVIĆ N M, JOVIĆEVIĆ N, STEVANOVIĆ J S, JOVIĆEVIĆ J N. Aluminium electrodeposition under novel conditions from $AlCl_3$–urea

deep eutectic solvent at room temperature [J]. Transactions of Nonferrous Metals Society of China, 2020, 30: 823−834.
[30] RANGARAJAN S K. Contribution to the theory of electrochemical phase formation [J]. Faraday Symposia of Chemical Society, 1977, 12: 101.
[31] SMITH E L, BARRON J C, ABBOTT A P, RYDER K S. Time resolved in situ liquid atomic force microscopy and simultaneous acoustic impedance electrochemical quartz crystal microbalance measurements: A study of Zn deposition [J]. Analytical Chemistry, 2009, 81: 8466−8471.
[32] WINN B, SHAPIRO S M, LASHEY J C, OPEIL C, RATCLIFF W. Structural phase transition in AuZn alloys [J]. Journal of Physics: Conference Series, 2010, 251: 012027.
[33] OKAMOTO B H, MASSALSKI T B. The Au−Zn (gold−zinc) system [J]. Bulletin of Alloy Phase Diagrams, 1989, 10: 59−69.
[34] JOVIĆEVIĆ N, CVETKOVIĆ V S, KAMBEROVIĆ Ž J, JOVIĆEVIĆ J N. Al−Zn alloy formation by aluminium underpotential deposition from $AlCl_3$+NaCl melts on zinc substrate [J]. International Journal of the Electrochemical Science, 2012, 7: 10380−10393.
[35] LEE J R I, O'MALLEY R L, O'CONNELL T J, VOLLMER A, RAYMENT T. X-ray absorption spectroscopy characterization of Zn underpotential deposition on Au(111) from phosphate supporting electrolyte [J]. Electrochimica Acta, 2010, 55: 8532−8538.

基于氯化胆碱的低共熔体系在 Au 上电沉积无枝晶 Zn

Vesna S. CVETKOVIĆ[1], Nebojša D. NIKOLIĆ[1],
Tanja S. BARUDŽIJA[2], Silvana B. DIMITRIJEVIĆ[3], Jovan N. JOVIĆEVIĆ[1]

1. Department of Electrochemistry, Institute of Chemistry, Technology and Metallurgy, University of Belgrade, Njegoševa 12, 11000 Belgrade, Serbia;
2. Institute for Nuclear Sciences Vinča, University of Belgrade, P.O. Box 522, 11001 Belgrade, Serbia;
3. Mining and Metallurgy Institute, Zeleni bulevar 35, 19210 Bor, Serbia

摘　要：以氯化胆碱和乙二醇混合液为低共熔溶剂，不使用其他添加剂，电化学沉积无枝晶 Zn/Au 合金。在不同的 Zn(II)浓度下，采用恒电位电沉积法在相对较低的 Zn 电沉积过电位下进行电沉积。通过循环伏安法(CV)和计时安培法(CA)揭示 Zn 电沉积的电化学机理。采用扫描电子显微镜和 X 射线衍射分析（XRD）对沉积层的形貌和结构进行表征，并用能谱仪对沉积层进行元素分析。CV 结果表明，Zn 的电沉积始于 Zn 欠电位沉积区，并一直持续到 Zn 过电位沉积(OPD)区。随着 Zn(II)浓度的增加，Zn/Zn(II) 电偶的沉积电位向更高的正值偏移。CA 分析表明，在 Zn 的 OPD 区开始三维渐进形核，随后形成三维生长。形貌分析表明，电沉积始于致密 Zn 岛的形成，随后形成无枝晶 Zn/Au 合金。 XRD 分析表明，其物相为金属 Zn、立方 $AuZn_3$ 和 AuZn 金属间化合物。

关键词：锌电沉积；低共熔溶剂；锌金合金；形貌；结构

(Edited by Bing YANG)